

Two-loop renormalization group calculation of response functions for a two-dimensional flat Fermi surface

Eberth Correa,^{1,*} Hermann Freire,² and Alvaro Ferraz¹

¹*Centro Internacional de Física da Matéria Condensada, Universidade de Brasília, Brasília 70904-970, Brazil*

²*Institut für Theoretische Physik, Universität Frankfurt, Max-von-Laue Strasse 1, 60438 Frankfurt, Germany*

(Received 26 December 2005; revised manuscript received 29 November 2006; published 10 November 2008)

We present the formalism for a two-loop renormalization group (RG) calculation of some order-parameter susceptibilities associated with a two-dimensional (2D) flat Fermi-surface model. In this order of perturbation theory, one must take into account the self-energy effects directly in all RG flow equations. In one-loop order, our calculation reproduces the well-known results obtained previously by other RG schemes. That is, for repulsive interactions all susceptibilities diverge in the low-energy limit and the antiferromagnetic (AF) spin-density-wave correlations produce indeed the leading instability in the system. In contrast, in two-loop order, only the AF susceptibility diverges for this model. However, even this divergence takes place at a much slower rate than in the one-loop RG approach. The purpose of this paper is to show in a very simple setting how to assess the importance of two-loop quantum fluctuations in 2D interacting fermionic models. With some modifications, the present formalism can also be extended to discuss more realistic models such as the paradigmatic 2D Hubbard model.

DOI: [10.1103/PhysRevB.78.195108](https://doi.org/10.1103/PhysRevB.78.195108)

PACS number(s): 71.27.+a, 71.10.Hf, 71.10.Pm

I. INTRODUCTION

Ever since the first appearance of the high- T_c superconductors, Anderson¹ argued that the electronic properties of those newly found compounds should be related to a two-dimensional (2D) electron-gas analog of a Luttinger-liquid-like behavior rather than to a conventional Fermi liquid. As is well known, in a one-dimensional (1D) lattice the strongly interacting electrons exhibit both a metallic Luttinger-liquid state away from half filling for $U > 0$, with explicit spin-charge separation effects, and a Mott-insulating regime at half filling. To study those systems in one dimension, successful methods were employed such as bosonization² and the Bethe ansatz.³ However, those schemes are either inapplicable or simply much too difficult to implement in higher dimensions. One approach which is equally successful in both one and higher dimensions is the renormalization group (RG) method. Several different RG schemes are already available for describing interacting electrons in the presence of a 2D Fermi surface (FS).^{4–18} Due to the complexity of the RG flow equations, the first RG results performed to discuss 2D interacting fermionic systems limited themselves to a thorough analysis of one-loop fluctuations effects. However, to discuss self-energy effects in the normal phase of the model, one needs to analyze two-loop order quantum fluctuations or beyond. Those effects will manifest themselves directly in the renormalization of the quasiparticle weight Z . In addition, both Luttinger-liquid-like behavior and Mott-insulating regime are signaled by the nullification of the quasiparticle weight. The renormalization of Z has been partially accounted for a 2D FS by other authors.^{16,19–23} In Ref. 6, the renormalization of Z at two loops is used to renormalize the fermionic one-particle Green's functions in the RG equation at one-loop order. However, this approximation is not conserving. This is due to the fact that if Z is taken up to two loops while the coupling constants continue to be considered up to one loop, they are not treated on equal footing. In view of that, such a scheme also violates the Ward identities. To

correct that scenario one should consider both Z and the coupling functions at least up to two-loop order. This has already been done elsewhere.^{24,25} Recently, Mastropietro²⁶ employed a nonperturbative method (the constructive field-theoretical method) which takes full account of the Ward identities to show the existence of a Luttinger line of fixed points for such a FS with a special choice of the external momenta for the scattering processes. Although his Hamiltonian model is slightly different from ours, this suffices to prove the importance of keeping the Ward identities well preserved order by order in perturbation theory.

In this work, we investigate how those effects affect the main physical instabilities of a perfectly nested two-dimensional truncated FS with rounded corners. This simple model avoids any considerations of Van Hove singularities which are present, for example, in the 2D Hubbard model near half filling. In addition, it allows us to calculate in an easy way all the two-loop diagrams which involve double integrals of the internal momenta in the k space. As demonstrated previously²⁵ in two-loop order, we have logarithmically divergent diagrams in the four-leg irreducible functions for the interactions, the so-called nonparquet diagrams. As we will see, those nonparquet diagrams by themselves strengthen the instability of density waves in the model. This occurs due to the fact that the most divergent couplings in the model, in either one loop or two loops, are precisely those in which the incoming momenta of the scattered particles are perfectly nested, that is, $\mathbf{p}_1 - \mathbf{p}_2 = \mathbf{Q}^*$ (nesting vector). As a result, in a self-consistent two-loop order calculation, they play a decisive role especially when the flatness of the FS is complete.

As it was demonstrated elsewhere¹⁷ in such a flat 2D FS, as soon as interactions are added to the model, the flow to strong coupling generates an instability of the Landau Fermi-liquid regime. This simple picture is improved by our two-loop approach. Here we put forward a scenario that this instability in fact indicates non-Fermi-liquid character which manifests itself in the suppression of the quasiparticle weight

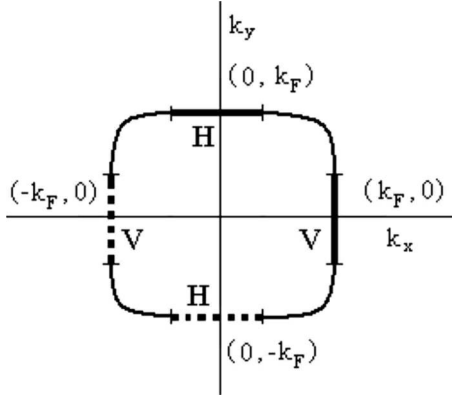


FIG. 1. The 2D flat Fermi surface with rounded corners. We divide it into four regions: two of the solid-line type and two of the dashed-line type.

as a function of the interaction.^{24,25} Here we discuss in detail how those results also influence directly the response functions of the physical system. In particular, all susceptibilities flow to fixed values with the exception of the antiferromagnetic (AF) susceptibility. However, even that unlimited growth takes place at a much slower rate than that observed in one-loop order. This is clear evidence that the main effect of the feedback of the quasiparticle weight into RG equations is to partially cancel out the existing divergences, making the flow, as a result, much slower.

The presentation of our results begins with the derivation of the corresponding RG equations for the vertex functions and the associated susceptibilities within our field-theory method. We discuss initially one-loop order results and show that they reproduce both the parquet¹⁷ and other fermionic RG schemes.^{6,15} Following this we present our two-loop results. We show that for initial positive values of the renormalized couplings of equal magnitude, the AF is indeed the leading instability in the physical system with all the others being strongly suppressed by the two-loop renormalization process. We conclude our work by discussing the physical meaning of our findings. Finally, we point out that extensions of the field-theory RG method to discuss more realistic models such as the 2D Hubbard model were also recently performed.²⁷

II. TWO-DIMENSIONAL FLAT FERMI-SURFACE MODEL

First of all, we consider a perfectly nested FS as shown in Fig. 1. For convenience and to keep a closer contact with well-known works in the literature, we divide the FS into four regions. In two of them, which we call horizontal (H), the parallel momentum to the surface is $-\Delta \leq p_x \leq \Delta$. In the other two, the vertical (V) ones, the parallel momentum varying along the FS is $-\Delta \leq p_y \leq \Delta$. The parallel momenta are restricted to vary only along those flat patches of the FS with 2Δ being essentially their size. Since we take a perfectly rigid FS, we neglect how the interactions renormalize the FS itself. It would be too complex to do otherwise at this stage. As a result, the momentum k_F will not be renormalized in our approach and we will simply assume its noninteracting

value. For the same reason, we will also neglect the Fermi velocity v_F momentum dependence along the FS. If we expand the one-particle energy $\varepsilon_a(\mathbf{p})$ around the Fermi momentum k_F , it now reduces to a linear dispersion, $\varepsilon_a(\mathbf{p}) = v_F(|p_\perp| - k_F)$, where v_F is the constant Fermi velocity and ε_a is measured with respect to the Fermi energy. Here $p_\parallel = p_x$ and $p_\perp = p_y$ for the H patches. Notice that this dispersion relation depends only on the momenta perpendicular to the Fermi surface, where the label $a = \pm$ refers to the flat sectors at $p_\perp = \pm k_F$. In doing so we only consider the flat parts whose nesting vectors are $\mathbf{Q}^* = (0, \pm 2k_F)$ for the H patches. If we were to consider the V patches instead, we would take $p_\perp = p_x$, $p_\parallel = p_y$, and $\mathbf{Q}^* = (\pm 2k_F, 0)$. In addition, we consider a fixed momentum cutoff λ which results in the interval $k_F - \lambda \leq |p_\perp| \leq k_F + \lambda$ for the perpendicular component in the vicinity of the FS.

In our RG method, only the marginally relevant processes are important for the RG flow²⁸ and therefore the marginally irrelevant scattering processes are not taken into account.⁴ As a result, only processes which produce the infrared (IR) logarithmically divergent contributions in a conventional perturbation theory must be considered. They are directly associated with a pair of parallel FS patches, either of H or V type, as well as between patches perpendicular to each other. This is due to the energy relation dispersion which depends only on the perpendicular component of the momentum in each flat region on the FS. This allows us to separate all the integrals in two parts: one related to the parallel part and another to the perpendicular one. Since we introduced the cutoff λ , all the couplings will acquire automatically a parallel momentum dependence in the RG procedure. Consequently, we are free to integrate analytically the perpendicular part of all the integrals that produce logarithmic divergences in the low-energy limit. Another consequence in considering such an energy relation dispersion is that the angular contribution on the FS for the energy is constant. In other words, in this model the density of states is constant.

Now we can introduce the marginally relevant processes considered in our model. They are displayed in Fig. 2, following the pedagogical presentation of Shankar⁴ for the available scattering processes and the well-known “g-ology” notation. Relating only horizontal patches on the FS, we have the backscattering [$g_1(\{p_\parallel\})$] and the forward-scattering [$g_2(\{p_\parallel\})$] processes; mixing horizontal and vertical patches of the flat FS, we have the BCS-scattering [$g^{\text{BCS}}(\{p_\parallel\})$] processes. We are not considering umklapp processes which are of two types: one relating horizontal patches on the FS and another mixing horizontal and vertical parts. As demonstrated by Zheleznyak *et al.*,¹⁷ within the parquet approximation, inclusion of the umklapp processes do not affect the main results for the susceptibilities. The $g_4(\{p_\parallel\})$ -scattering processes are also marginally relevant but are not considered here for simplicity. In one dimension such a process is responsible for the renormalization of the single-particle Fermi velocity and for spin-charge separation effects. Since we want to study the effects of the two-loop quantum fluctuations into the RG equations in a simple setting, we will neglect this kind of process for the moment.

Since we showed in detail elsewhere²⁵ all the necessary steps to perform the renormalization of this 2D flat FS model

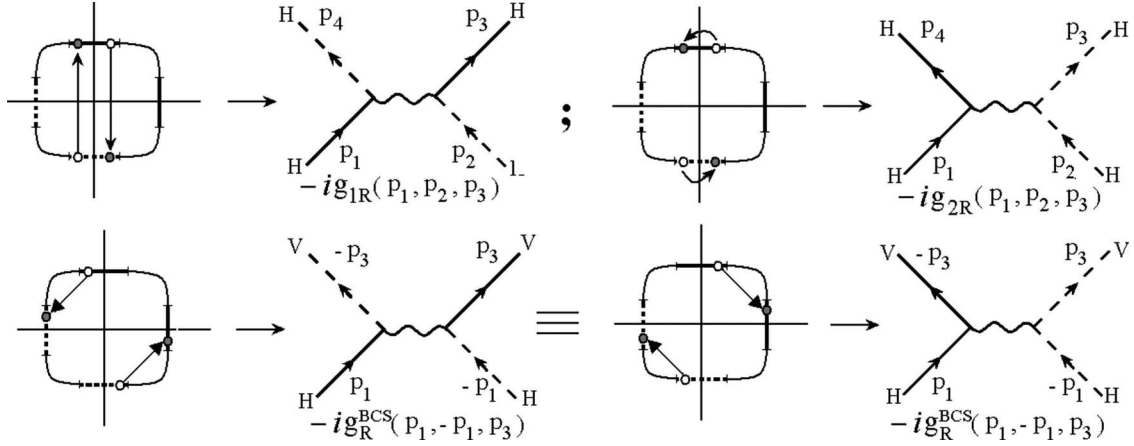


FIG. 2. The interaction processes of the initial model and the corresponding Feynman rules for the vertices. The g_{1R} , g_{2R} , and g_R^{BCS} couplings stand for the renormalized backscattering, forward scattering, and BCS scattering, respectively. The two BCS-type processes displayed are equivalent to each other.

up to two-loop order, we rewrite the renormalized Lagrangian L entirely in terms of the renormalized fields and couplings, i.e.,

$$\begin{aligned}
 L = & \sum_{\substack{\mathbf{p}, \sigma, a = \pm \\ j = H, V}} Z \psi_{R(a)\sigma}^{\dagger}(\mathbf{p}) [i\partial_t - v_F(|p_{\perp}| - k_F)] \psi_{R(a)\sigma}^j(\mathbf{p}) \\
 & - \frac{1}{V} \sum_{\alpha, \beta} \sum_{\substack{j = H, V \\ \gamma, \delta \in \{\mathbf{p}_i\}}} \left[\prod_{i=1}^4 Z(p_{i\parallel}) \right]^{1/2} [g_{2B} \delta_{\alpha\delta} \delta_{\beta\gamma} - g_{1B} \delta_{\alpha\gamma} \delta_{\beta\delta}] \\
 & \times \psi_{R(+)\delta}^{\dagger}(\mathbf{p}_4) \psi_{R(-)\gamma}^{\dagger}(\mathbf{p}_3) \psi_{R(-)\beta}^j(\mathbf{p}_2) \psi_{R(+)\alpha}^j(\mathbf{p}_1) \\
 & - \frac{1}{V} \sum_{\alpha, \beta} \sum_{\substack{j = H, V \\ \gamma, \delta \in \{\mathbf{p}_i\}}} \left[\prod_{i=1}^4 Z(p_{i\parallel}) \right]^{1/2} g_B^{\text{BCS}} \\
 & \times [\delta_{\alpha\delta} \delta_{\beta\gamma} - \delta_{\alpha\gamma} \delta_{\beta\delta}] [\psi_{R(+)\delta}^{\dagger}(\mathbf{p}_4) \psi_{R(-)\gamma}^{\dagger}(\mathbf{p}_3) \\
 & \times \psi_{R(-)\beta}^H(\mathbf{p}_2) \psi_{R(+)\alpha}^H(\mathbf{p}_1) \delta_{\mathbf{p}_1 + \mathbf{p}_2, 0} \delta_{\mathbf{p}_3 + \mathbf{p}_4, 0} + \text{H.c.}]. \quad (2.1)
 \end{aligned}$$

Here the $\psi_{R(\pm)}^{\dagger H(V)}$ and $\psi_{R(\pm)}^H(V)$ are, respectively, the creation and annihilation fermion field operators for particles located at the horizontal (vertical) \pm patches. The couplings g_{1B} , g_{2B} , and g_B^{BCS} stand for bare backscattering, forward-scattering, and BCS-scattering couplings, respectively. They are related to their renormalized associates by

$$g_{iB} = \left[\prod_{i=1}^4 Z(p_{i\parallel}) \right]^{-1/2} [g_{iR}(p_{1\parallel}, p_{2\parallel}, p_{3\parallel}) + \Delta g_{iR}(p_{1\parallel}, p_{2\parallel}, p_{3\parallel})]. \quad (2.2)$$

From now on we will consider the thermodynamic limit ($V \rightarrow \infty$) with all momenta summations becoming integrals such as $\sum_{\mathbf{p}} \rightarrow V \int d^2\mathbf{p} / (2\pi)^2$. The diagrammatic representations of the corresponding renormalized forward-scattering, backscattering, and BCS interactions are shown schematically in Fig. 2. Although the two types of BCS couplings shown in that figure seem to be different at first sight, they are indeed equivalent to each other in the sense that they

produce identical contributions. In all Feynman diagrams, the noninteracting single-particle propagators $G_{(+)}^{(0)}$ and $G_{(-)}^{(0)}$ are represented by a solid and a dashed line, respectively, following their association with the corresponding FS patches.

We review briefly the main results of our RG analysis for a flat 2D FS before we deal directly with the response functions. In Sec. III, we summarize the main results of the field-theory RG for the quasiparticle weight and the renormalized coupling functions as well as the corresponding RG equations.

III. RENORMALIZED COUPLING FUNCTIONS AND SELF-ENERGY UP TO TWO LOOPS

A. Self-energy and quasiparticle weight up to two loops

As we mentioned before, in two-loop order another quantity plays an important role in the RG equations for the renormalized couplings: the quasiparticle weight Z . The renormalization of Z basically characterizes the interaction regime. This effect reflects itself in an important way in the RG equations for the renormalized coupling functions²⁵ and, as we will see next, in the response functions. To calculate Z we must determine the renormalized self-energy Σ_R . Figure 3 displays the self-energy diagrams for the determination of Z up to two-loop order. The so-called sunset diagrams produce logarithmic singularities multiplied by the factor $[p_0$

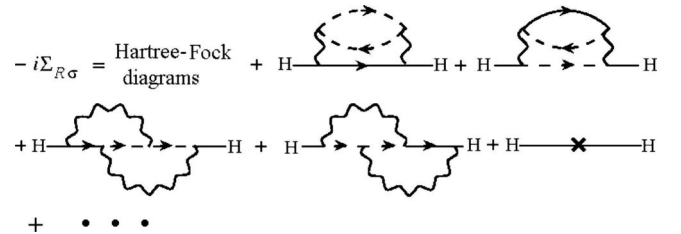


FIG. 3. The self-energy diagrams up to two loops. The sunset diagrams will cause the renormalization of the quasiparticle weight Z .

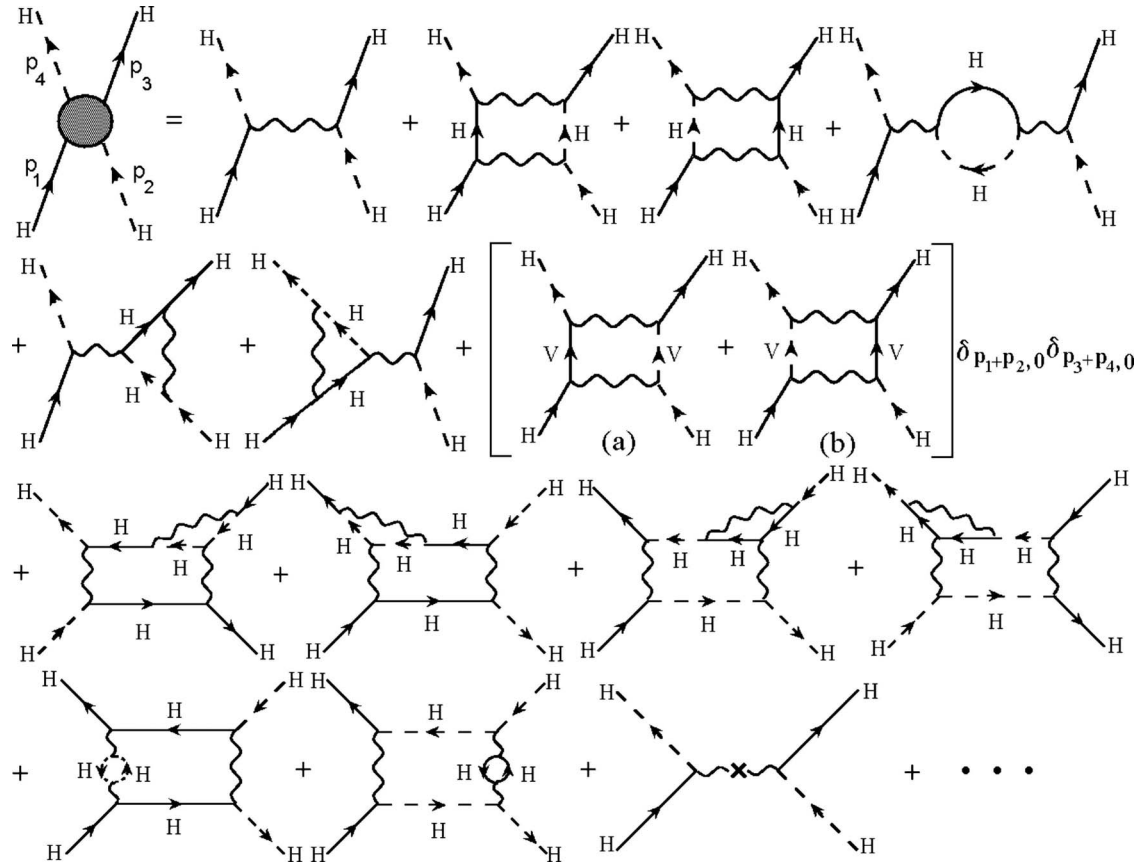


FIG. 4. The diagrams for the renormalized four-point vertex in the backscattering channel up to two loops. The single-particle propagators are represented by either a solid or a dashed line (H type) according to their association with the corresponding FS patches. The last diagram stands for the counterterm.

$-v_F(|p_y| - k_F)$ which can only be canceled out by the corresponding counterterm diagram associated with the multiplicative fermion field factor Z . The use of an appropriate RG prescription for the one-particle Green's function at $p_y = \pm k_F$ together with those contributions leads to the determination of Z . It then follows that the quasiparticle weight satisfies the RG equation

$$\omega \frac{\partial Z(p_{\parallel}; \omega)}{\partial \omega} = \gamma(p_{\parallel}) Z(p_{\parallel}; \omega), \quad (3.1)$$

where $\gamma(p_{\parallel})$ is the anomalous dimension and ω is the energy scale which denotes the proximity of the renormalized theory to the FS. The full expression for γ is given in Appendix A. The numerical estimates of Z follow our previous work. As we will observe later, the suppression of the quasiparticle weight as we go beyond the weak-coupling limit changes dramatically the one-loop scenario.

B. Two-loop RG equations for the renormalized couplings

In Eq. (2.1) we wrote the renormalized Lagrangian which will automatically generate renormalized physical quantities in perturbation theory at any loop order. As a result, applying suitable Feynman rules one can arrive at the diagrams shown in Figs. 4–6. The last diagrams in the sets are the counterterms which render the theory finite. Most of the diagrams in

Figs. 4 and 5 were already calculated elsewhere.²⁵ The diagrams that appear between square brackets are due to the BCS contributions and their respective expressions can be found in Appendix C. The counterterm of the BCS channel in Fig. 6 can be also found in Appendix C. In what follows, we identify the renormalized one-particle irreducible $\Gamma_{iR}^{(4)}$ ($i = 1, 2$) such that, at the FS, the corresponding renormalized coupling functions $g_{iR}(p_{1\parallel}, p_{2\parallel}, p_{3\parallel}; \omega)$ are given by

$$\Gamma_{iR}^{(4)}(p_1, p_2, p_3)|_{\text{FS}} = -i g_{iR}(p_{1\parallel}, p_{2\parallel}, p_{3\parallel}; \omega). \quad (3.2)$$

Taking into account the associated Z factors for the external momenta and the RG conditions $dg_{iB}/d\omega = 0$ for the bare coupling functions, the RG equations of the coupling functions follow immediately,

$$\omega \frac{dg_{iR}(p_{1\parallel}, p_{2\parallel}, p_{3\parallel})}{d\omega} = \frac{1}{2} \sum_{j=1}^4 \gamma(p_{j\parallel}) g_{iR}(p_{1\parallel}, p_{2\parallel}, p_{3\parallel}) - \omega \frac{\partial \Delta g_{iR}(p_{1\parallel}, p_{2\parallel}, p_{3\parallel})}{\partial \omega}, \quad (3.3)$$

where $i = 1, 2, \text{BCS}$. We make use of the numerical estimates of those RG equations in the calculations presented in this work. Once we do that, we are ready to implement the RG strategy to calculate the renormalized response vertices. This will be done in what follows.

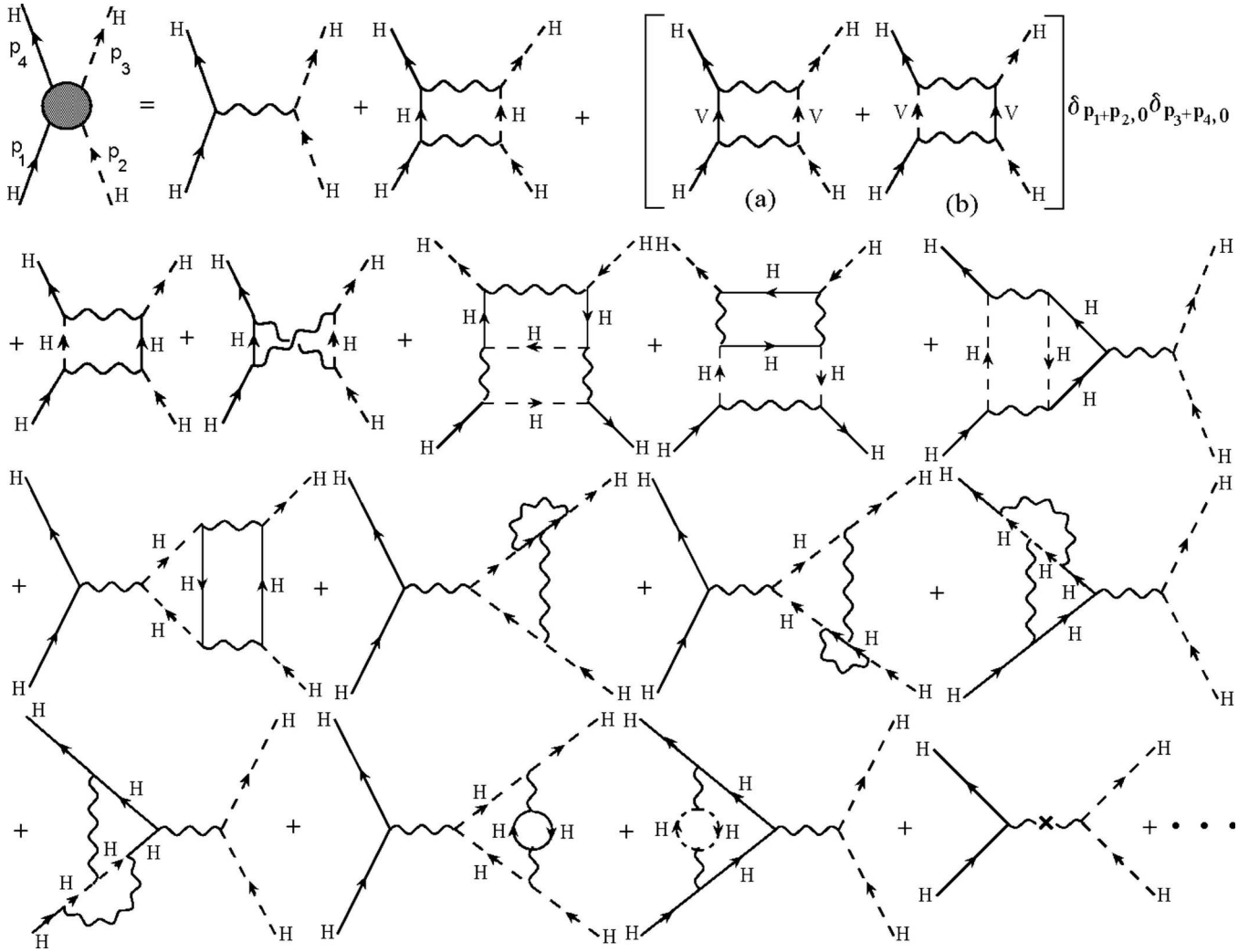


FIG. 5. The diagrams for the renormalized four-point vertex in the forward-scattering channel up to two loops. The last diagram stands for the counterterm.

IV. RESPONSE FUNCTIONS

Following the RG strategy for studying the pairing and density-wave instabilities of the system, let us add initially to the renormalized Lagrangian of the system two *fictitious* infinitesimal external fields h_{SC} (for the pairing term) and h_{DW} (for the density wave), which act essentially as source fields for the generation of particle-particle and particle-hole pairs. That is, we add to our renormalized Lagrangian the contributions

$$\begin{aligned}
 L_{ext} = & -\frac{1}{V} \sum_{\mathbf{k}, \mathbf{q}} [Z^{1/2}(k_{\parallel})Z^{1/2}(q_{\parallel} - k_{\parallel})h_{SC}(\mathbf{q})\mathcal{T}_{SC}^{B\alpha\beta}(\mathbf{k}, \mathbf{q}) \\
 & \times \psi_{R(+)\alpha}^{\dagger H}(\mathbf{k})\psi_{R(-)\beta}^{\dagger H}(\mathbf{q} - \mathbf{k}) + Z^{1/2}(k_{\parallel})Z^{1/2}(k_{\parallel} - q_{\parallel}) \\
 & \times h_{DW}(\mathbf{q})\mathcal{T}_{DW}^{B\alpha\beta}(\mathbf{k}, \mathbf{q})\psi_{R(+)\alpha}^{\dagger H}(\mathbf{k})\psi_{R(-)\beta}^H(\mathbf{k} - \mathbf{q}) + \text{H.c.}], \quad (4.1)
 \end{aligned}$$

where $\mathcal{T}_i^{B\alpha\beta}(\mathbf{k}, \mathbf{q})$ ($i=SC, DW$) is the *bare* response vertex. As we explained before, we will consider again the thermo-

dynamic limit with all momenta summations becoming integrals. By means of the added Lagrangian L_{ext} , we are now able to generate the one-particle irreducible functions associated with the composite pairing and the composite particle-hole operators. Since we are interested in the response functions for the density-wave and superconductor channels, we

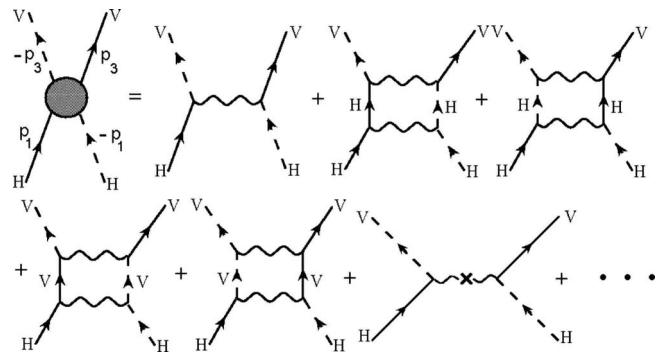


FIG. 6. The diagrams for the renormalized four-point vertex in the BCS channel. The last diagram corresponds to the counterterm.

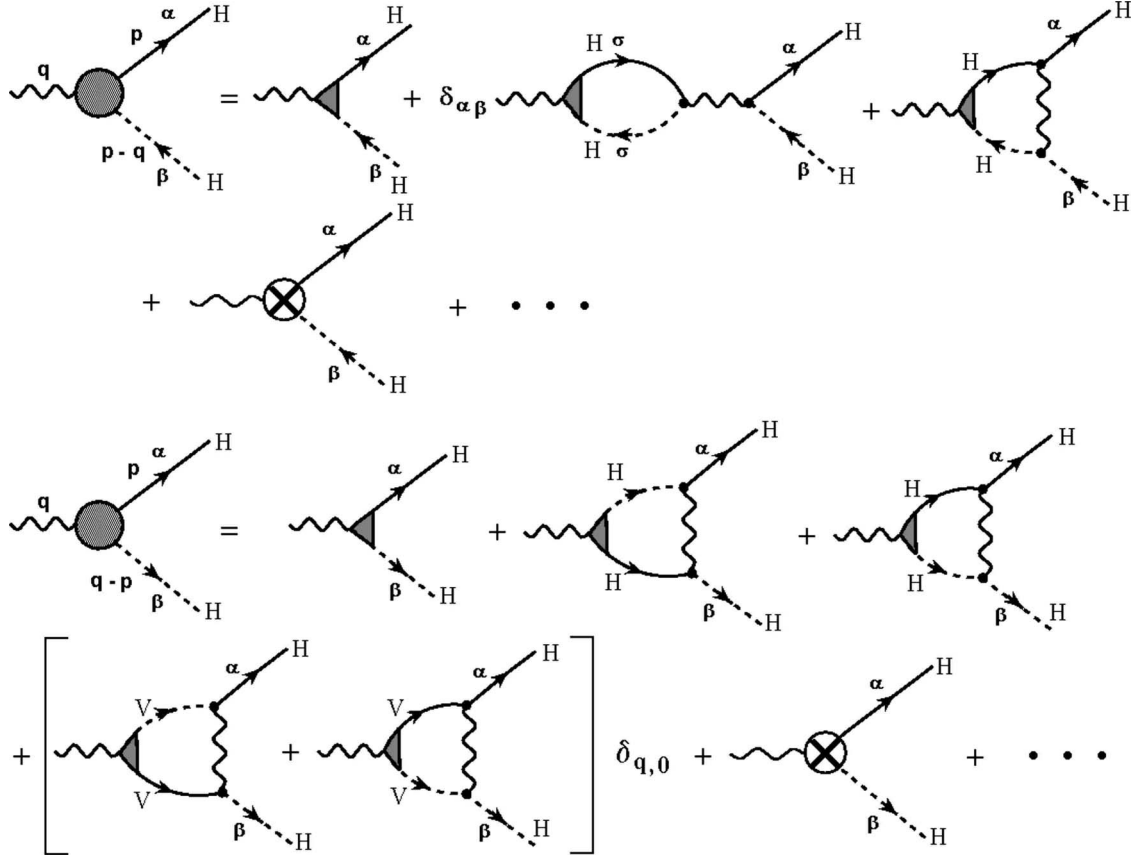


FIG. 7. The Feynman diagrams up to one-loop order for the renormalized response vertices $\mathcal{T}_{DW}^{R\alpha\beta}$ (density-wave channel) and $\mathcal{T}_{SC}^{R\alpha\beta}$ (superconducting channel).

need to define the associated three-point generalized Green's functions, namely, $G_{DW\alpha\beta}^{R(2,1)}$ and $G_{SC\alpha\beta}^{R(2,1)}$. In doing this we obtain the corresponding $\Gamma_{DW\alpha\beta}^{R(2,1)}$ and $\Gamma_{SC\alpha\beta}^{R(2,1)}$ by cutting out the external legs of the corresponding $G_i^{R(2,1)}$'s. Here the $G_i^{R(2,1)}$'s are given by

$$G_{DW\alpha\beta}^{R(2,1)}(p, q) = i \frac{\delta}{\delta h_{DW}(\mathbf{q})} \left\langle \psi_{R(+)\alpha}^\dagger(\mathbf{p}) \psi_{R(-)\beta}(\mathbf{p} - \mathbf{q}) \times \exp \left[i \int_{q_0 p_0} L_{\text{ext}} \right] \right\rangle_{h_{DW}=h_{SC}=0} \quad (4.2)$$

and

$$G_{SC\alpha\beta}^{R(2,1)}(p, q) = i \frac{\delta}{\delta h_{SC}(\mathbf{q})} \left\langle \psi_{R(+)\alpha}^\dagger(\mathbf{p}) \psi_{R(-)\beta}^\dagger(\mathbf{q} - \mathbf{p}) \times \exp \left[i \int_{q_0 p_0} L_{\text{ext}} \right] \right\rangle_{h_{DW}=h_{SC}=0}, \quad (4.3)$$

where $\langle \dots \rangle$ stands for $\int \mathcal{D}\psi \mathcal{D}\psi^\dagger \exp iS[\psi, \psi^\dagger](\dots)$, with S being the classical action associated with the renormalized Lagrangian given by Eq. (2.1).

Following conventional Feynman rules, we display the diagrams in Fig. 7 for the density-wave and superconducting channels up to one-loop order. Notice that there are no other logarithmically divergent diagrams in $\Gamma_R^{(2,1)}$. Consequently, in

our scheme the resulting higher-loop effects in our two-loop order calculation for the response vertices are produced by the Z factors and the renormalized couplings in the RG equations. Hence, if we consider the external Lagrangian in Eq. (4.1), we can rewrite the *bare* response vertices such that

$$\mathcal{T}_{DW}^{B\alpha\beta}(\mathbf{p}, \mathbf{q}) = Z^{-1/2}(p_{\parallel}, \omega) Z^{-1/2}(p_{\parallel} - q_{\parallel}, \omega) \times [\mathcal{T}_{DW}^{R\alpha\beta}(\mathbf{p}, \mathbf{q}) + \Delta \mathcal{T}_{DW}^{R\alpha\beta}(\mathbf{p}, \mathbf{q})], \quad (4.4)$$

$$\mathcal{T}_{SC}^{B\alpha\beta}(\mathbf{p}, \mathbf{q}) = Z^{-1/2}(p_{\parallel}, \omega) Z^{-1/2}(q_{\parallel} - p_{\parallel}, \omega) \times [\mathcal{T}_{SC}^{R\alpha\beta}(\mathbf{p}, \mathbf{q}) + \Delta \mathcal{T}_{SC}^{R\alpha\beta}(\mathbf{p}, \mathbf{q})]. \quad (4.5)$$

The counterterm $\Delta \mathcal{T}_{DW(SC)}^{R\alpha\beta}$ guarantees the cancellation of the divergent vertex functions diagrams in one-loop order. This renders the theory finite at the FS. Notice that the renormalized response vertices depend on the momenta \mathbf{p} and \mathbf{q} . Now, we are ready to set up the prescriptions for the renormalized one-particle irreducible Green's functions $\Gamma_{Ri\alpha\beta}^{(2,1)}$ in terms of experimentally observable physical quantities, i.e.,

$$\Gamma_{DW\alpha\beta}^{R(2,1)}(p_{\parallel}, p_{\perp} = k_F, p_0; q_{\parallel}, q_{\perp} = 2k_F, q_0 = \omega) = -i \mathcal{T}_{DW}^{R\alpha\beta}(p_{\parallel}, q_{\parallel}; \omega), \quad (4.6)$$

$$\Gamma_{SC\alpha\beta}^{R(2,1)}(p_{\parallel}, p_{\perp} = k_F, p_0; q_{\parallel}, q_{\perp} = 0, q_0 = \omega) = -i\mathcal{T}_{SC}^{R\alpha\beta}(p_{\parallel}, q_{\parallel}; \omega). \quad (4.7)$$

As we already mentioned, all renormalized quantities depend on ω (RG scale). However, to avoid overloading notations we omit this dependence from now on except when it is strictly necessary to do so. In this way, considering the diagrams shown in Fig. 7 and making use of the RG conditions stated in Eqs. (4.6) and (4.7), we arrive at

$$\begin{aligned} \Delta\mathcal{T}_{DW}^{R\alpha\beta} &= \frac{1}{4\pi^2v_F} \int_{\mathcal{D}_1} dk_{\parallel} \left[\delta_{\alpha\beta} \sum_{\sigma=\uparrow\downarrow} g_{1R}(k_{\parallel}, p_{\parallel} - q_{\parallel}, p_{\parallel}) \right. \\ &\quad \times \mathcal{T}_{DW}^{R\sigma\sigma}(k_{\parallel}, q_{\parallel}) - g_{2R}(k_{\parallel}, p_{\parallel} - q_{\parallel}, p_{\parallel}) \\ &\quad \left. \times \mathcal{T}_{DW}^{R\alpha\beta}(k_{\parallel}, q_{\parallel}) \right] \ln\left(\frac{\Omega}{\omega}\right), \end{aligned} \quad (4.8)$$

$$\begin{aligned} \Delta\mathcal{T}_{SC}^{R\alpha\beta} &= \frac{1}{4\pi^2v_F} \int_{\mathcal{D}_2} dk_{\parallel} [g_{2R}(k_{\parallel}, q_{\parallel} - k_{\parallel}, q_{\parallel} - p_{\parallel}) \\ &\quad \times \mathcal{T}_{SC}^{R\alpha\beta}(k_{\parallel}, q_{\parallel}) - g_{1R}(k_{\parallel}, q_{\parallel} - k_{\parallel}, p_{\parallel}) \mathcal{T}_{SC}^{R\beta\alpha}(k_{\parallel}, q_{\parallel})] \ln\left(\frac{\Omega}{\omega}\right) \\ &\quad + \frac{\delta_{q_x,0}}{4\pi^2v_F} \int_{\mathcal{D}_{10}} dk_y [g_R^{\text{BCS}}(k_y, -k_y + q_x, -p_x + q_x) \\ &\quad \times \mathcal{T}_{SC}^{R\alpha\beta}(k_y, q_x) - g_R^{\text{BCS}}(k_y, -k_y + q_x, p_x) \\ &\quad \times \mathcal{T}_{SC}^{R\beta\alpha}(k_y, q_x)] \ln\left(\frac{\Omega}{\omega}\right). \end{aligned} \quad (4.9)$$

Taking into account the fact that the *bare* quantities do not know anything about the RG scale, we can differentiate Eqs. (4.4) and (4.5) with respect to ω to get

$$\begin{aligned} \omega \frac{d}{d\omega} \mathcal{T}_{DW}^{R\alpha\beta}(p_{\parallel}, q_{\parallel}) &= -\omega \frac{d}{d\omega} \Delta\mathcal{T}_{DW}^{R\alpha\beta}(p_{\parallel}, q_{\parallel}) + \frac{1}{2} \mathcal{T}_{DW}^{R\alpha\beta}(p_{\parallel}, q_{\parallel}) \\ &\quad \times [\gamma(p_{\parallel}, \omega) + \gamma(p_{\parallel} - q_{\parallel}, \omega)], \end{aligned} \quad (4.10)$$

$$\begin{aligned} \omega \frac{d}{d\omega} \mathcal{T}_{SC}^{R\alpha\beta}(p_{\parallel}, q_{\parallel}) &= -\omega \frac{d}{d\omega} \Delta\mathcal{T}_{SC}^{R\alpha\beta}(p_{\parallel}, q_{\parallel}) + \frac{1}{2} \mathcal{T}_{SC}^{R\alpha\beta}(p_{\parallel}, q_{\parallel}) \\ &\quad \times [\gamma(p_{\parallel}, \omega) + \gamma(q_{\parallel} - p_{\parallel}, \omega)], \end{aligned} \quad (4.11)$$

where γ is again the anomalous dimension, which reflects the self-energy feedback into these RG equations.

Consistently with the renormalized density-wave and pairing response vertices $\mathcal{T}_{DW}^{R\alpha\beta}$ and $\mathcal{T}_{SC}^{R\alpha\beta}$, we can now do the symmetrization with respect to the spin components to define

$$\mathcal{T}_{CDW}^R(p_{\parallel}, q_{\parallel}) = \mathcal{T}_{DW}^{R\uparrow\uparrow}(p_{\parallel}, q_{\parallel}) + \mathcal{T}_{DW}^{R\downarrow\downarrow}(p_{\parallel}, q_{\parallel}), \quad (4.12)$$

$$\mathcal{T}_{SDW}^R(p_{\parallel}, q_{\parallel}) = \mathcal{T}_{DW}^{R\uparrow\downarrow}(p_{\parallel}, q_{\parallel}) - \mathcal{T}_{DW}^{R\downarrow\uparrow}(p_{\parallel}, q_{\parallel}), \quad (4.13)$$

$$\mathcal{T}_{SSC}^R(p_{\parallel}, q_{\parallel}) = \mathcal{T}_{SC}^{R\uparrow\downarrow}(p_{\parallel}, q_{\parallel}) - \mathcal{T}_{SC}^{R\downarrow\uparrow}(p_{\parallel}, q_{\parallel}), \quad (4.14)$$

$$\mathcal{T}_{TSC}^R(p_{\parallel}, q_{\parallel}) = \mathcal{T}_{SC}^{R\uparrow\downarrow}(p_{\parallel}, q_{\parallel}) + \mathcal{T}_{SC}^{R\downarrow\uparrow}(p_{\parallel}, q_{\parallel}), \quad (4.15)$$

where CDW refers to charge-density wave, SDW to spin-density wave, SSC to singlet superconductivity, and TSC to triplet superconductivity.

Since we have already defined the symmetrized renormalized response vertices with respect to spin projection, we are now able to write down their corresponding RG equations,

$$\begin{aligned} \omega \frac{d}{d\omega} \mathcal{T}_b^R(p_{\parallel}, q_{\parallel}) &= -\omega \frac{d}{d\omega} \Delta\mathcal{T}_b^R(p_{\parallel}, q_{\parallel}) + \frac{1}{2} \mathcal{T}_b^R(p_{\parallel}, q_{\parallel}) \\ &\quad \times [\gamma(p_{\parallel}, \omega) + \gamma(p_{\parallel} - q_{\parallel}, \omega)], \end{aligned} \quad (4.16)$$

$$\begin{aligned} \omega \frac{d}{d\omega} \mathcal{T}_c^R(p_{\parallel}, q_{\parallel}) &= -\omega \frac{d}{d\omega} \Delta\mathcal{T}_c^R(p_{\parallel}, q_{\parallel}) + \frac{1}{2} \mathcal{T}_c^R(p_{\parallel}, q_{\parallel}) \\ &\quad \times [\gamma(p_{\parallel}, \omega) + \gamma(q_{\parallel} - p_{\parallel}, \omega)], \end{aligned} \quad (4.17)$$

where $b=CDW, SDW$ and $c=SSC, TSC$. The full expressions for the symmetrized counterterms $\Delta\mathcal{T}_i^R$ for the anomalous dimension are given in Appendix A. Due to the particular shape of our flat FS, the renormalized couplings must be symmetrical with respect to the exchange of upper (right) and lower (left) particles and the change of sign of the external p_{ix} 's. It then follows from that

$$\begin{aligned} g_{iR}(p_{1\parallel}, p_{2\parallel}, p_{3\parallel}) &= g_{iR}(-p_{1\parallel}, -p_{2\parallel}, -p_{3\parallel}), \\ g_{iR}(p_{1\parallel}, p_{2\parallel}, p_{3\parallel}) &= g_{iR}(p_{2\parallel}, p_{1\parallel}, p_{4\parallel}), \\ g_{iR}(p_{1\parallel}, p_{2\parallel}, p_{3\parallel}) &= g_{iR}(p_{4\parallel}, p_{3\parallel}, p_{2\parallel}). \end{aligned} \quad (4.18)$$

All those symmetries are implicit in the Lagrangian model. The first is the symmetry with respect to time inversion. The second is the permutation symmetry and, finally, the last one is the hermiticity symmetry. These conditions are necessary for the RG equations to produce the correct numerical results when we approach the FS. These symmetries are satisfied by Eqs. (4.16) and (4.17), which are symmetrical with respect to the sign reversal of p_{\parallel} for a fixed q_{\parallel} . Following this we can therefore define two irreducible representations of this symmetry which never mix with each other, namely,

$$\mathcal{T}_b^{R\pm}(p_{\parallel}, q_{\parallel}) = \mathcal{T}_b^R(p_{\parallel}, q_{\parallel}) \pm \mathcal{T}_b^R(-p_{\parallel}, q_{\parallel}), \quad (4.19)$$

$$\mathcal{T}_c^{R\pm}(p_{\parallel}, q_{\parallel}) = \mathcal{T}_c^R(p_{\parallel}, q_{\parallel}) \pm \mathcal{T}_c^R(-p_{\parallel}, q_{\parallel}), \quad (4.20)$$

where again $b=CDW, SDW$ and $c=SSC, TSC$. The (+) sign is associated with the *s*-wave symmetry, whereas the (-) sign is associated with the *d*-wave symmetry instead. Now, considering the symmetries of the couplings in Eq. (4.18) and the new symmetrized response vertices in Eqs. (4.19) and (4.20), we can write RG equations (4.16) and (4.17) in the following way:

$$\begin{aligned} \omega \frac{d}{d\omega} \mathcal{T}_b^{R\pm}(p_{\parallel}, q_{\parallel}) &= -\omega \frac{d}{d\omega} \Delta\mathcal{T}_b^{R\pm}(p_{\parallel}, q_{\parallel}) + \frac{1}{2} \mathcal{T}_b^{R\pm}(p_{\parallel}, q_{\parallel}) \\ &\quad \times [\gamma(p_{\parallel}, \omega) + \gamma(p_{\parallel} - q_{\parallel}, \omega)], \end{aligned} \quad (4.21)$$

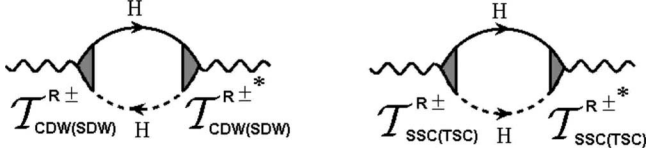


FIG. 8. The Feynman diagrams corresponding to the susceptibilities associated with the renormalized response vertices $\mathcal{T}_{\text{CDW(SDW)}}^{R\pm}$ and $\mathcal{T}_{\text{SSC(TSC)}}^{R\pm}$.

$$\omega \frac{d}{d\omega} \mathcal{T}_c^{R\pm}(p_{\parallel}, q_{\parallel}) = -\omega \frac{d}{d\omega} \Delta \mathcal{T}_c^{R\pm}(p_{\parallel}, q_{\parallel}) + \frac{1}{2} \mathcal{T}_c^{R\pm}(p_{\parallel}, q_{\parallel}) \times [\gamma(p_{\parallel}, \omega) + \gamma(q_{\parallel} - p_{\parallel}, \omega)], \quad (4.22)$$

where the expressions for $\Delta \mathcal{T}_{\text{CDW}}^{R\pm}$, $\Delta \mathcal{T}_{\text{SDW}}^{R\pm}$, $\Delta \mathcal{T}_{\text{SSC}}^{R\pm}$, and $\Delta \mathcal{T}_{\text{TSC}}^{R\pm}$ can be found in Appendix B. The plus sign in the DWs' response vertices is associated with the charge- and spin-density waves. However, the minus-sign symmetry of the parallel momentum along the FS in those DWs yield circular charge (spin) currents flowing around the square lattice with alternating directions. In this way we associate this symmetry of the DWs with the charge- and spin-current waves also known as flux phases. Once the renormalized $\mathcal{T}_{\text{CDW(SDW)}}^{R\pm}$ and $\mathcal{T}_{\text{SSC(TSC)}}^{R\pm}$ are found, we can define the related susceptibilities following the diagrammatic scheme shown in Fig. 8. As one can see there is an IR-divergent *bubble* in each channel. The explicit calculation of those two logarithmic divergent bubbles can be found in our previous work.²⁵ We arrive immediately at the RG equations for the various susceptibilities,

$$\omega \frac{d}{d\omega} \chi_b^{R\pm}(q_{\parallel}, \omega) = \frac{1}{4\pi^2 v_F} \int_{\mathcal{D}_3} dp_{\parallel} [\mathcal{T}_b^{R\pm}(p_{\parallel}, q_{\parallel})]^* \mathcal{T}_b^{R\pm}(p_{\parallel}, q_{\parallel}), \quad (4.23)$$

$$\omega \frac{d}{d\omega} \chi_c^{R\pm}(q_{\parallel}, \omega) = \frac{1}{4\pi^2 v_F} \int_{\mathcal{D}_4} dp_{\parallel} [\mathcal{T}_c^{R\pm}(p_{\parallel}, q_{\parallel})]^* \mathcal{T}_c^{R\pm}(p_{\parallel}, q_{\parallel}), \quad (4.24)$$

where \mathcal{D}_3 and \mathcal{D}_4 are the intervals determined in Appendix B and b and c refer to the symmetries mentioned before. Those expressions are written in general form. However, since we are not considering Umklapp processes, it turns out that $\mathcal{T}_{b,c}^{R\pm} = (\mathcal{T}_{b,c}^{R\pm})^*$.

V. NUMERICAL RESULTS

In order to solve all the RG equations, we have to resort to numerical methods. More specifically, as we emphasized before we want to estimate how the susceptibilities change as we vary the scale ω in order to take the physical system toward the low-energy limit. As we did in an earlier work,²⁵ we discretize here the FS continuum replacing the interval $-\Delta \leq p_{\parallel} \leq \Delta$ by a discrete set of 33 points in each patch. For convenience, we use $\omega = \Omega \exp(-l)$, where $\Omega = 2v_F \lambda$ is a fixed ultraviolet (i.e., microscopic) cutoff with l being our RG step. We choose $\Omega/v_F \Delta = 1$. In view of our choice of

points to represent the whole FS, we are only allowed to go up to $l \approx 2.8$ in the RG flow. The reason for that is to avoid the distance ω to the FS becoming smaller than the distance between adjacent points since the discretization procedure would no longer apply for this case.

The RG equations for all couplings considered here were obtained in Sec. III. In order to integrate them numerically, all of Eqs. (3.1), (3.3), and (4.21)–(4.24) have to be solved simultaneously. Hence, the numerical procedure becomes much more involved technically.

The choices of the initial conditions at $l=0$ in the RG equations are, in principle, arbitrary. This is related to the fact that one may choose any microscopic model to start with in order to study its low-energy properties. Since we are most interested in the repulsive case, we initially set the couplings as $\bar{g}_{1R} = \bar{g}_{2R} = \bar{g}_R^{\text{BCS}} = 8$, where $\bar{g}_R = g_R / \pi v_F$.

In order to reproduce the symmetries of the order parameters with respect to the FS, we choose the following initial conditions (i.e., $l=0$) for the response vertices:

$$\mathcal{T}_{\text{CDW}}^{R+}(p_{\parallel}, q_{\parallel}) = \mathcal{T}_{\text{SDW}}^{R+}(p_{\parallel}, q_{\parallel}) = \mathcal{T}_{\text{SSC}}^{R+}(p_{\parallel}, q_{\parallel}) = \mathcal{T}_{\text{TSC}}^{R+}(p_{\parallel}, q_{\parallel}) = 1, \quad (5.1)$$

$$\begin{aligned} \mathcal{T}_{\text{CDW}}^{R-}(p_{\parallel}, q_{\parallel}) &= \mathcal{T}_{\text{SDW}}^{R-}(p_{\parallel}, q_{\parallel}) = \mathcal{T}_{\text{SSC}}^{R-}(p_{\parallel}, q_{\parallel}) \\ &= \mathcal{T}_{\text{TSC}}^{R-}(p_{\parallel}, q_{\parallel}) = \sqrt{2} \sin\left(\frac{\pi p_{\parallel}}{2\Delta}\right). \end{aligned} \quad (5.2)$$

We call attention to the fact that despite the initial values of the response vertices being either unity or a function of p_{\parallel} , the q_{\parallel} dependence will be generated naturally by the renormalization process. The choice made for the symmetrized (+) vertices is motivated by their independence with respect to the change of sign of p_{\parallel} . In contrast, for the antisymmetric vertices (−), our choice is oriented by our need to reproduce the well-known symmetries of the so-called flux phases and the $d_{x^2-y^2}$ superconductivity with respect to the FS. Those symmetries are particularly relevant for the high- T_c cuprates. Furthermore, we take all susceptibilities equal to zero at $l=0$, that is, $\chi_i^{\pm}(q_{\parallel}; l=0) = 0$ (for $i = \text{CDW, SDW, SSC, TSC}$). This is motivated by the fact that at the microscopic scale there is no order.

As we will see next, it will emerge from our numerical estimates that the AF susceptibility produces the leading instability when the transfer momentum is equal to the nesting vector ($\mathbf{q} = \mathbf{Q}^*$). To make the comparison of our results with previous estimates found in the literature, we display our computations in two steps. Initially, we show the one-loop order results since they can be compared directly with calculations presented by other groups. Next, we move on to display our two-loop calculations. Following that, we discuss the most interesting results and the difference between our estimates in one loop and two loops.

A. One-loop RG approach

The one-loop results for all susceptibilities with initial values of $\bar{g}_{1R} = \bar{g}_{2R} = \bar{g}_R^{\text{BCS}} = 8$ are displayed in Fig. 9. As it can be seen, all susceptibilities seem to diverge but the leading one is the AF (i.e., SDW+) susceptibility in such a repulsive

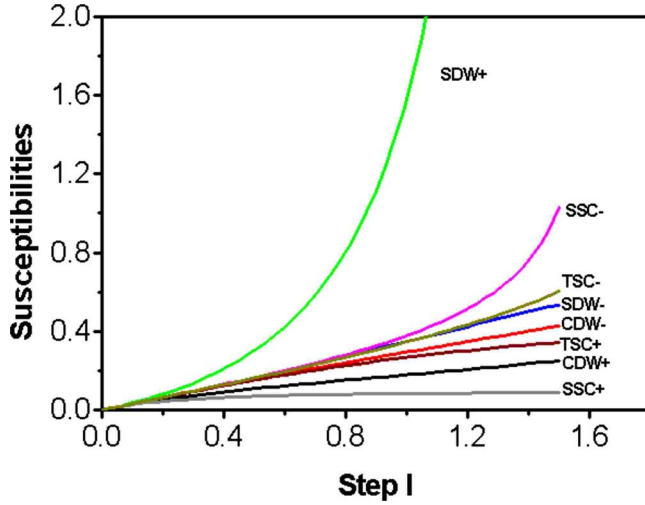


FIG. 9. (Color online) The RG flows of the susceptibilities $\chi_i^+(q_{\parallel}=0; l)$ versus the step l in the one-loop approach; the numerical results with $\bar{g}_{1R}=\bar{g}_{2R}=\bar{g}_R^{\text{BCS}}=8$ as initial conditions for the couplings. The AF (i.e., SDW+) susceptibility diverges for $l \approx 1.5$.

regime. According to this, we should expect an antiferromagnetic spin-density-wave ground state and no sign of unconventional metallic behavior in the physical system for this regime. In addition, the second most pronounced renormalized susceptibility corresponds to a $d_{x^2-y^2}$ -wave singlet superconductivity (i.e., SSC-). This result is in good agreement with several RG studies concerning the 2D repulsive case when the flatness of the FS becomes more evident.^{6,12,15–18} We find numerically that all the BCS couplings, regardless of the choice of the external momenta, flow to zero in the low-energy limit. This is, in particular, consistent with Ref. 18. The physical reason for that is the perfect nesting of our fixed FS, which tends to suppress these interaction processes involving perpendicular FS patches in our model.

Another point which deserves comment here concerns the one-loop RG flows of the renormalized backscattering [$g_{1R}(\{p_{\parallel}\})$] and forward-scattering [$g_{2R}(\{p_{\parallel}\})$] couplings as we approach the low-energy limit in this system. These interaction processes are known to diverge (or, equivalently, to flow toward a strong-coupling regime) for several choices of external momenta. This was explicitly shown in our earlier work²⁵ and, for this reason, we only discuss here the most important points. At the one-loop level, the quasiparticle weight Z is always taken equal to unity throughout the RG calculation. In order to investigate possible non-Fermi-liquid regimes, this situation must be contrasted with other scenarios, in which Z might approach zero as well. As we mentioned before, the renormalization of Z can be only achieved if we implement a two-loop (or beyond) RG scheme. For this reason, we move on to the main goal of this work, which is to analyze what is the precise two-loop feedback of the quasiparticle renormalization into all RG flow equations of the system. More specifically, we want to discuss to what extent the two-loop results change the one-loop scenario. This will be done in what follows.

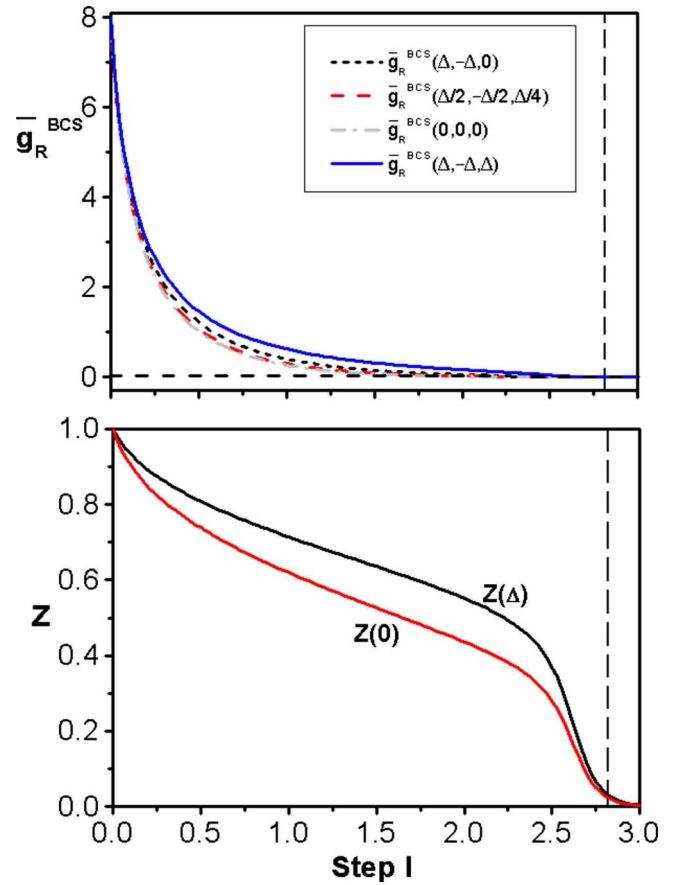


FIG. 10. (Color online) The RG flows of the BCS couplings (upper panel) and the quasiparticle weight (lower panel) for some choices of momenta in the two-loop approach. As initial conditions, we take $\bar{g}_{1R}=\bar{g}_{2R}=\bar{g}_R^{\text{BCS}}=8$ and $Z=1$. The dashed line stands for $l=2.8$.

B. Two-loop RG approach

Now, we turn to the case we are most interested in, i.e., the full two-loop RG approach. As we mentioned before, we have to solve Eqs. (4.21)–(4.24) simultaneously with the RG equations for the renormalized couplings [Eq. (3.3)] using the initial conditions given by Eqs. (5.1) and (5.2), $\chi_i^+(q_{\parallel}; l=0)=0$ and $\bar{g}_{1R}=\bar{g}_{2R}=\bar{g}_R^{\text{BCS}}=8$, respectively.

First of all, we display the RG flows of the BCS couplings and the quasiparticle weight Z for some choices of momenta in Fig. 10. Note that after a strong renormalization of the quasiparticle weight Z , the BCS couplings flow even more strongly to zero. Hence we can conclude that for our perfectly nested FS, in the repulsive regime, such BCS processes do not affect significantly our RG estimates. In addition, the RG flows of the backscattering [$g_{1R}(\{p_{\parallel}\})$] and forward scattering [$g_{2R}(\{p_{\parallel}\})$] are shown in Fig. 11. We obtain that as soon as the Z effects become important, the rate of change in the couplings reduces abruptly. Although the couplings seem to reach a plateau regime, they now in fact change their values continuously at a very slow rate. Moreover, in view of the fact that those plateau values are very sensitive to the discretization procedure, we cannot associate these results with the existence of stable IR fixed points. This

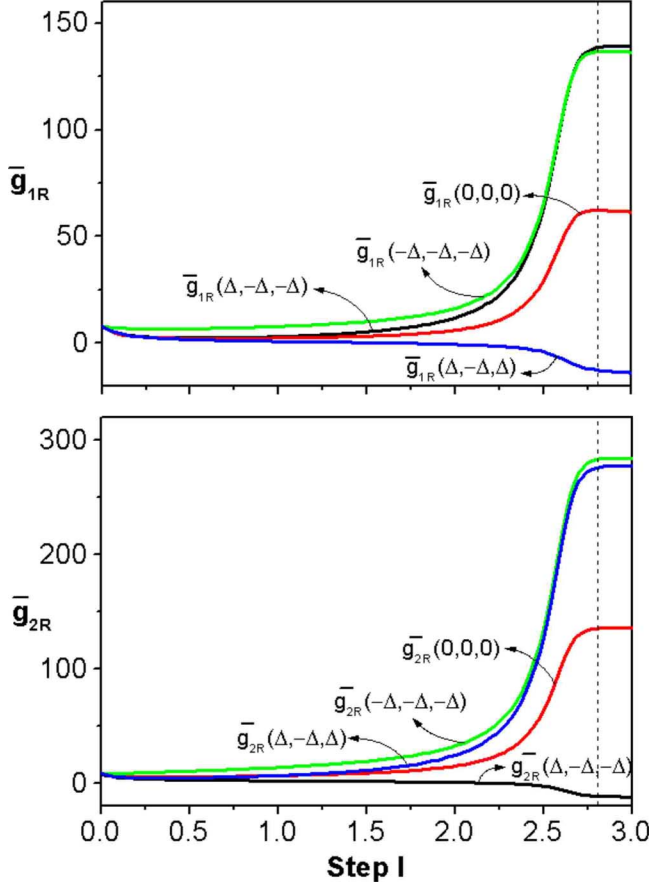


FIG. 11. (Color online) The RG flows for the backscattering (upper panel) and forward scattering (lower panel) up to two loops with $\bar{g}_{1R}=\bar{g}_{2R}=\bar{g}_R^{\text{BCS}}=8$ as initial conditions. The dashed line represents $l=2.8$.

point was already discussed in our earlier work.²⁵ This fact reveals the limitation of the perturbative methods employed to solve such models. Now, we move on to analyze the key role played by the suppression of Z into the behavior of the susceptibilities in two-loop order.

The results obtained for the susceptibilities (with the exception of the AF susceptibility) are shown in Fig. 12. As one can see in this figure, the feedback of the self-energy up to two loops in the RG equations changes drastically the one-loop scenario. It is interesting to note that the plateau values appear at $l \approx 2.7$ for almost all susceptibilities. This is precisely the RG scale where the strong renormalization of the quasiparticle weight Z takes place. In contrast with the scenario obtained for the coupling functions at the same two-loop order, these plateaus are real fixed values since they are not sensitive to our FS discretization procedure. Thus, we can infer from this result that, with the exception of the AF instability, all existing order tendencies tend to become suppressed by the self-energy effects and to manifest themselves at most as *short-range* correlations.

On the other hand, concerning the RG flow of the AF susceptibility, this situation is unfortunately much more subtle. This susceptibility in fact continues to diverge even in the two-loop approach. Notwithstanding that, this divergence takes place at a much slower rate than that observed in one-

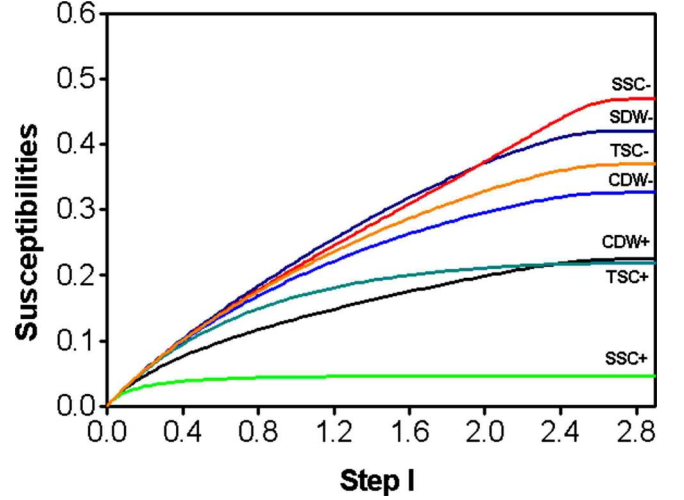


FIG. 12. (Color online) The RG flows of the susceptibilities with the exception of SDW+ symmetry for $q_{\parallel}=0$ in the two-loop approach with $\bar{g}_{1R}=\bar{g}_{2R}=\bar{g}_R^{\text{BCS}}=8$ as initial conditions.

loop order. This result is shown explicitly in Fig. 13 for $q_{\parallel}=0$. Indeed, we can observe from this figure that, as we move from one loop to two loops, this divergence occurs at a lower-energy critical scale ω_c (or, equivalently, a larger critical RG step l_c). As a result, it seems reasonable to expect that if we added higher-order quantum fluctuations (as, e.g., in a three-loop RG calculation or beyond), this divergence would occur at even lower critical energy scales. As a result, in the exact theory such a divergence would be correctly restricted to $T=0$.

VI. CONCLUSION

In the present work, we performed a full two-loop RG calculation of the susceptibilities associated with the order-parameters CDW, SDW, SSC, and TSC of s -wave and d -wave symmetries for a 2D flat FS model. In this toy model, we considered only the following parametrized interactions: the backscattering [$g_{1R}(\{p_{\parallel}\})$], the forward-

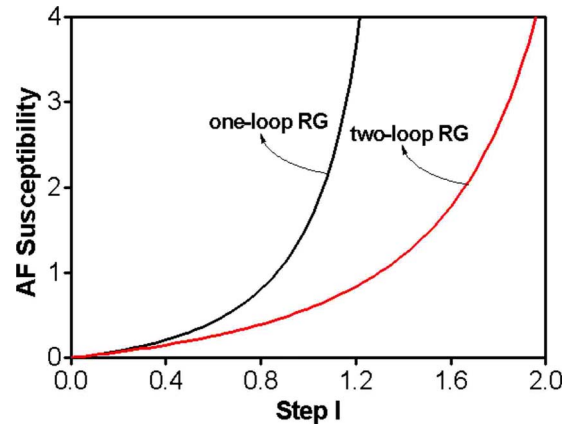


FIG. 13. (Color online) The AF (i.e., SDW+) susceptibilities $\chi_{\text{SDW}^+}^+(q_{\parallel}=0; l)$ in one-loop and two-loop orders with $\bar{g}_{1R}=\bar{g}_{2R}=\bar{g}_R^{\text{BCS}}=8$ as initial conditions.

scattering $[g_{2R}(\{p_{i\parallel}\})]$, and the BCS couplings $[g_R^{\text{BCS}}(\{p_{i\parallel}\})]$. We neglected the umklapp effects at this stage since they are not expected to change significantly the main results for the susceptibilities in such a FS, as explicitly shown by Zheleznyak *et al.*¹⁷ in their one-loop RG approach. As is well known this model possesses several logarithmic divergences in the low-energy limit within the conventional perturbation-theory scheme. To render the theory finite we applied the RG field-theory method by defining appropriate counterterms order by order in perturbation theory.

Due to the particular shape of our FS, we are able to reproduce some symmetries by choosing appropriate initial conditions for the renormalized response vertices. The shape of such a FS is kept fixed and never changes throughout our calculations. Nevertheless the general expectation was that the resulting low-energy physical state would have several competing instabilities such as the so-called flux phases (CDW- and SDW-), the d -wave singlet superconductivity (SSC-), the d -wave triplet superconductivity (TSC-), the s -wave singlet superconductivity (SSC+), the triplet superconductivity of s type (TSC+), the AF spin-density wave (SDW+), and the charge-density wave (CDW+). In one-loop order, all these susceptibilities diverge in the low-energy limit. The leading instability is the AF of s type and the second strongest instability is the $d_{x^2-y^2}$ -wave singlet superconductivity, in good agreement with other RG studies.^{17,18}

In two-loop order, as the self-energy feedback is fully taken into account in all RG equations, we obtain that all susceptibilities flow to fixed values with the exception of the AF instability, which continues to diverge in that case. The second most pronounced susceptibility is the $d_{x^2-y^2}$ -wave singlet superconductivity, which in fact flows to a *plateau* value. This is produced by the strong suppression produced by the quasiparticle weight Z , which is associated with either a Mott-insulating or a non-Fermi-liquid regime. In this sense, we can conclude that for such a perfectly nested FS the self-energy feedback goes against the $d_{x^2-y^2}$ -wave singlet superconductivity. We should however be cautious of the existence of divergent susceptibilities at nonzero RG scales. The divergence in two-loop order takes place at larger values of the RG step l in comparison with what is obtained in one-loop order. It is therefore reasonable to expect that in higher orders the divergence only takes place at even higher l values. This is in agreement with the general expectation that strong quantum fluctuations should be a dominant feature in such a 2D model.

Summarizing our results, we showed here in detail how the self-energy effects reflect themselves in the susceptibilities associated with the leading instabilities of a 2D Fermi gas with a perfectly flat FS. By keeping well preserved the Ward identities in two-loop order, we can see that the self-energy effects suppress the $d_{x^2-y^2}$ -wave singlet superconductivity for this 2D flat FS. This is a direct consequence of the nullification of the quasiparticle weight associated with the flatness of the FS. However we were not able to find fixed points for this model even considering only the forward-scattering processes. Such fixed points as is well known could characterize the Luttinger-liquid-like regime. Nevertheless, we must call attention to the fact that our RG scheme has a perturbative nature and on top of that we

are not considering the $g_4(\{p_{i\parallel}\})$ -scattering processes, unlike Mastropietro,²⁶ who, using his constructive RG method, found those fixed points for such a FS.

To conclude, we showed that with the exception of the AF instability all other density waves and pairing instabilities are suppressed in this toy model. This is due to the fact that for a perfectly flat FS the nonparquet diagrams strengthen the spin-density-wave fluctuations, mainly the s -SDW type (or SDW+), and the flow of Z to zero is very effective in suppressing all the other instabilities as shown in this work. In more realistic models, such as the Hubbard model with a flat FS, the effects due to the Van Hove points and the umklapp processes must necessarily be included in the calculations. However, these effects indeed act to strengthen the spin-density-wave fluctuations close to half filling²⁹ even further. Consequently, as demonstrated in our results, one can expect a much slower growth rate for the flow for the $d_{x^2-y^2}$ -wave singlet superconductivity close to half filling when these new ingredients are added to our toy model. In contrast one can also expect the opposite trend for the s -SDW-type instability. We tested these assertions in another work.²⁷ Considering the Hubbard model with a varying doping parameter, we showed that in the vicinity of half filling, with a lightly doped FS, the self-energy effects indeed suppress the $d_{x^2-y^2}$ -wave singlet superconductivity, in qualitative good agreement with the directions pointed out in this work. Moreover, when the FS curvature destroys the perfect nesting, the self-energy effects are not so effective in suppressing the $d_{x^2-y^2}$ -wave singlet superconductivity. Those outcomes suggest that this simple toy model is indeed a good starting point for the study of electronic properties in the presence of flat Fermi surfaces. It is quite clear from our results that two-loop quantum fluctuations must be fully taken into account in the presence of such a FS ingredient.

ACKNOWLEDGMENTS

This work was partially supported by the Conselho Nacional de Desenvolvimento Científico e Tecnológico (CNPq), the Financiadora de Estudos e Projetos (FINEP), and the Ministry of Science and Technology (MCT).

APPENDIX A

In this appendix, we write down the explicit form of the ΔT_i^R 's with i =CDW,SDW,SSC,TSC and γ 's which are taken into account in Eqs. (4.16), (4.17), (4.21), and (4.22). We also give the several intervals of integration that are considered throughout this work. They are the following:

$$\mathcal{D}_1 = \begin{cases} -\Delta \leq k_{\parallel} \leq \Delta \\ -\Delta \leq p_{\parallel} \leq \Delta \\ -2\Delta \leq q_{\parallel} \leq 2\Delta \\ -\Delta \leq p_{\parallel} - q_{\parallel} \leq \Delta, \end{cases} \quad (\text{A1})$$

$$\mathcal{D}_2 = \begin{cases} -\Delta \leq k_{\parallel} \leq \Delta \\ -\Delta \leq p_{\parallel} \leq \Delta \\ -2\Delta \leq q_{\parallel} \leq 2\Delta \\ -\Delta \leq q_{\parallel} - k_{\parallel} \leq \Delta \\ -\Delta \leq q_{\parallel} - p_{\parallel} \leq \Delta, \end{cases} \quad (\text{A2})$$

$$\mathcal{D}_3 = \begin{cases} -\Delta \leq p_{\parallel} \leq \Delta \\ -2\Delta \leq q_{\parallel} \leq 2\Delta \\ -\Delta \leq p_{\parallel} - q_{\parallel} \leq \Delta, \end{cases} \quad (\text{A3})$$

$$\mathcal{D}_4 = \begin{cases} -\Delta \leq p_{\parallel} \leq \Delta \\ -2\Delta \leq q_{\parallel} \leq 2\Delta \\ -\Delta \leq q_{\parallel} - p_{\parallel} \leq \Delta, \end{cases} \quad (\text{A4})$$

$$\mathcal{D}_5 = \begin{cases} -\Delta \leq k_{\parallel} \leq \Delta \\ -\Delta \leq p_{\parallel} \leq \Delta \\ -\Delta \leq q_{1\parallel} \leq \Delta \\ -\Delta \leq -k_{\parallel} + p_{\parallel} + q_{1\parallel} \leq \Delta, \end{cases} \quad (\text{A5})$$

$$\mathcal{D}_6 = \begin{cases} -\Delta \leq k_{\parallel} \leq \Delta \\ -\Delta \leq p_{\parallel} \leq \Delta \\ -2\Delta \leq q_{\parallel} \leq 2\Delta \\ -\Delta \leq q_{1\parallel} \leq \Delta \\ -\Delta \leq -k_{\parallel} + p_{\parallel} - q_{\parallel} + q_{1\parallel} \leq \Delta, \end{cases} \quad (\text{A6})$$

$$\mathcal{D}_7 = \begin{cases} -\Delta \leq k_{\parallel} \leq \Delta \\ -2\Delta \leq q_{\parallel} \leq 2\Delta \\ -\Delta \leq p_{\parallel} \leq \Delta \\ -\Delta \leq q_{1\parallel} \leq \Delta \\ -\Delta \leq -k_{\parallel} + q_{\parallel} - p_{\parallel} + q_{1\parallel} \leq \Delta, \end{cases} \quad (\text{A7})$$

$$\mathcal{D}_8 = \begin{cases} -\Delta \leq k_x \leq \Delta \\ -\Delta \leq k_y \leq \Delta \\ -\Delta \leq p_{1x} \leq \Delta \\ -\Delta \leq p_{3y} \leq \Delta, \end{cases} \quad (\text{A8})$$

$$\mathcal{D}_9 = \begin{cases} -\Delta \leq k_y \leq \Delta \\ -\Delta \leq p_{1x} \leq \Delta \\ -\Delta \leq p_{3x} \leq \Delta, \end{cases} \quad (\text{A9})$$

$$\mathcal{D}_{10} = \begin{cases} -\Delta \leq k_y \leq \Delta \\ -\Delta \leq p_x \leq \Delta. \end{cases} \quad (\text{A10})$$

We begin with the expressions for the $\Delta\mathcal{T}_i^R$'s associated with $\Gamma^{(2,1)}$'s. We get

$$\begin{aligned} \Delta\mathcal{T}_{\text{CDW}}^R(p_{\parallel}, q_{\parallel}) &= \frac{1}{4\pi^2 v_F} \ln\left(\frac{\Omega}{\omega}\right) \int_{\mathcal{D}_1} dk_{\parallel} [2g_{1R}(k_{\parallel}, p_{\parallel} - q_{\parallel}, p_{\parallel}) \\ &\quad - g_{2R}(k_{\parallel}, p_{\parallel} - q_{\parallel}, k_{\parallel} - q_{\parallel})] \mathcal{T}_{\text{CDW}}^R(k_{\parallel}, q_{\parallel}), \end{aligned} \quad (\text{A11})$$

$$\begin{aligned} \Delta\mathcal{T}_{\text{SDW}}^R(p_{\parallel}, q_{\parallel}) &= -\frac{1}{4\pi^2 v_F} \ln\left(\frac{\Omega}{\omega}\right) \int_{\mathcal{D}_1} dk_{\parallel} g_{2R}(k_{\parallel}, p_{\parallel} - q_{\parallel}, k_{\parallel} \\ &\quad - q_{\parallel}) \mathcal{T}_{\text{SDW}}^R(k_{\parallel}, q_{\parallel}), \end{aligned} \quad (\text{A12})$$

$$\begin{aligned} \Delta\mathcal{T}_{\text{SSC}}^R(p_{\parallel}, q_{\parallel}) &= \frac{1}{4\pi^2 v_F} \ln\left(\frac{\Omega}{\omega}\right) \left\{ \int_{\mathcal{D}_2} dk_{\parallel} [g_{1R}(k_{\parallel}, -k_{\parallel} + q_{\parallel}, p_{\parallel}) \right. \\ &\quad + g_{2R}(k_{\parallel}, -k_{\parallel} + q_{\parallel}, -p_{\parallel} + q_{\parallel})] \mathcal{T}_{\text{SSC}}^R(k_{\parallel}, q_{\parallel}) \\ &\quad + \delta_{q_x, 0} \int_{\mathcal{D}_{10}} dk_y [g_R^{\text{BCS}}(k_y, -k_y + q_x, p_x) \\ &\quad + g_R^{\text{BCS}}(k_y, -k_y + q_x, -p_x + q_x)] \mathcal{T}_{\text{SSC}}^R(k_y, q_x) \left. \right\}, \end{aligned} \quad (\text{A13})$$

and finally

$$\begin{aligned} \Delta\mathcal{T}_{\text{TSC}}^R(p_{\parallel}, q_{\parallel}) &= -\frac{1}{4\pi^2 v_F} \ln\left(\frac{\Omega}{\omega}\right) \left\{ \int_{\mathcal{D}_2} dk_{\parallel} [g_{1R}(k_{\parallel}, -k_{\parallel} + q_{\parallel}, p_{\parallel}) \right. \\ &\quad - g_{2R}(k_{\parallel}, -k_{\parallel} + q_{\parallel}, -p_{\parallel} + q_{\parallel})] \mathcal{T}_{\text{TSC}}^R(k_{\parallel}, q_{\parallel}) \\ &\quad + \delta_{q_x, 0} \int_{\mathcal{D}_{10}} dk_y [g_R^{\text{BCS}}(k_y, -k_y + q_x, p_x) \\ &\quad - g_R^{\text{BCS}}(k_y, -k_y + q_x, -p_x + q_x)] \mathcal{T}_{\text{TSC}}^R(k_y, q_x) \left. \right\}. \end{aligned} \quad (\text{A14})$$

The anomalous dimension γ used in our RG equations for the renormalized response vertices is given by²⁵

$$\begin{aligned} \gamma(p_{\parallel}; \omega) &= \frac{1}{32\pi^4 v_F^2} \int_{\mathcal{D}_5} dk_{\parallel} dq_{1\parallel} [2g_{1R}(-k_{\parallel} + p_{\parallel} + q_{1\parallel}, k_{\parallel}, q_{1\parallel}) 2 \\ &\quad \times g_{1R}(p_{\parallel}, q_{1\parallel}, k_{\parallel}) + 2g_{2R}(p_{\parallel}, q_{1\parallel}, -k_{\parallel} + p_{\parallel} + q_{1\parallel}) g_{2R}(k_{\parallel}, \\ &\quad - k_{\parallel} + p_{\parallel} + q_{1\parallel}, q_{1\parallel}) - g_{1R}(p_{\parallel}, q_{1\parallel}, k_{\parallel}) g_{2R}(k_{\parallel}, -k_{\parallel} + p_{\parallel} \\ &\quad + q_{1\parallel}, q_{1\parallel}) - g_{2R}(p_{\parallel}, q_{1\parallel}, -k_{\parallel} + p_{\parallel} + q_{1\parallel}) g_{1R}(k_{\parallel}, -k_{\parallel} \\ &\quad + p_{\parallel} + q_{1\parallel}, p_{\parallel})]. \end{aligned} \quad (\text{A15})$$

APPENDIX B

Considering the symmetries obeyed by the coupling functions, we get the symmetrized (\pm) renormalized response vertices whose counterterms $\Delta\mathcal{T}_i^{\text{R}\pm}$ are given by

$$\begin{aligned} \Delta\mathcal{T}_{\text{CDW}}^{\text{R}\pm}(p_{\parallel}, q_{\parallel}) &= \frac{1}{4\pi^2 v_F} \ln\left(\frac{\Omega}{\omega}\right) \int_{\mathcal{D}_1} dk_{\parallel} [2g_{1R}(k_{\parallel}, p_{\parallel} - q_{\parallel}, p_{\parallel}) \\ &\quad - g_{2R}(k_{\parallel}, p_{\parallel} - q_{\parallel}, k_{\parallel} - q_{\parallel})] \mathcal{T}_{\text{CDW}}^{\text{R}\pm}(k_{\parallel}, q_{\parallel}), \end{aligned} \quad (\text{B1})$$

$$\begin{aligned} \Delta\mathcal{T}_{\text{SDW}}^{\text{R}\pm}(p_{\parallel}, q_{\parallel}) &= -\frac{1}{4\pi^2 v_F} \ln\left(\frac{\Omega}{\omega}\right) \int_{\mathcal{D}_1} dk_{\parallel} g_{2R}(k_{\parallel}, p_{\parallel} - q_{\parallel}, k_{\parallel} - q_{\parallel}) \\ &\quad \times \mathcal{T}_{\text{SDW}}^{\text{R}\pm}(k_{\parallel}, q_{\parallel}), \end{aligned} \quad (\text{B2})$$

$$\begin{aligned} \Delta \mathcal{T}_{\text{SSC}}^{R\pm}(p_{\parallel}, q_{\parallel}) = & \frac{1}{4\pi^2 v_F} \ln\left(\frac{\Omega}{\omega}\right) \left[\int_{\mathcal{D}_2} dk_{\parallel} [g_{1R}(k_{\parallel}, -k_{\parallel} + q_{\parallel}, p_{\parallel}) \right. \\ & + g_{2R}(k_{\parallel}, -k_{\parallel} + q_{\parallel}, -p_{\parallel} + q_{\parallel})] \mathcal{T}_{\text{SSC}}^{R\pm}(k_{\parallel}, q_{\parallel}) \\ & + \delta_{q_x, 0} \int_{\mathcal{D}_{10}} dk_y [g_R^{\text{BCS}}(k_y, -k_y + q_x, p_x) \\ & \left. + g_R^{\text{BCS}}(k_y, -k_y + q_x, -p_x + q_x)] \mathcal{T}_{\text{SSC}}^{R\pm}(k_y, q_x) \right], \end{aligned} \quad (\text{B3})$$

and finally

$$\begin{aligned} \Delta \mathcal{T}_{\text{TSC}}^{R\pm}(p_{\parallel}, q_{\parallel}) = & -\frac{1}{4\pi^2 v_F} \ln\left(\frac{\Omega}{\omega}\right) \left[\int_{\mathcal{D}_2} dk_{\parallel} [g_{1R}(k_{\parallel}, -k_{\parallel} + q_{\parallel}, p_{\parallel}) \right. \\ & - g_{2R}(k_{\parallel}, -k_{\parallel} + q_{\parallel}, -p_{\parallel} + q_{\parallel})] \mathcal{T}_{\text{TSC}}^{R\pm}(k_{\parallel}, q_{\parallel}) \\ & + \delta_{q_x, 0} \int_{\mathcal{D}_{10}} dk_y [g_R^{\text{BCS}}(k_y, -k_y + q_x, p_x) \\ & \left. - g_R^{\text{BCS}}(k_y, -k_y + q_x, -p_x + q_x)] \mathcal{T}_{\text{TSC}}^{R\pm}(k_y, q_x) \right]. \end{aligned} \quad (\text{B4})$$

APPENDIX C

In this appendix, we will present all the expressions in which the BCS coupling must be considered. We start with the counterterm in the BCS channel which gives simply

$$\begin{aligned} \Delta g_R^{\text{BCS}} = & \frac{1}{4\pi^2 v_F} \ln\left(\frac{\Omega}{\omega}\right) \left\{ + \int_{\mathcal{D}_8} dk_x [g_R^{\text{BCS}}(p_{1x}, -p_{1x}, -k_x) g_R^{\text{BCS}}(k_x, \right. \\ & - k_x, p_{3y}) + g_R(p_{1x}, -p_{1x}, k_x) g_R^{\text{BCS}}(-k_x, k_x, p_{3y})] \\ & \times \int_{\mathcal{D}_8} dk_y [g_R(k_y, -k_y, p_{3y}) g_R^{\text{BCS}}(p_{1x}, -p_{1x}, -k_y) \\ & \left. + g_R(-k_y, k_y, p_{3y}) g_R^{\text{BCS}}(p_{1x}, -p_{1x}, k_y)] \right\}. \end{aligned} \quad (\text{C1})$$

In the following, we present the contributions of the BCS coupling into the other channels showed in Figs. 4 and 5, which are given by

$$\begin{aligned} \Gamma_{1R(a)}^{(4)} = & \frac{i}{4\pi^2 v_F} \ln\left(\frac{\Omega}{\omega}\right) \int_{\mathcal{D}_9} dk_y g_R^{\text{BCS}}(p_{1x}, -p_{1x}, -k_y) \\ & \times g_R^{\text{BCS}}(k_y, -k_y, p_{3x}), \end{aligned} \quad (\text{C2})$$

$$\begin{aligned} \Gamma_{1R(b)}^{(4)} = & \frac{i}{4\pi^2 v_F} \ln\left(\frac{\Omega}{\omega}\right) \int_{\mathcal{D}_9} dk_y g_R^{\text{BCS}}(p_{1x}, -p_{1x}, k_y) \\ & \times g_R^{\text{BCS}}(-k_y, k_y, p_{3x}), \end{aligned} \quad (\text{C3})$$

$$\begin{aligned} \Gamma_{2R(a)}^{(4)} = & \frac{i}{4\pi^2 v_F} \ln\left(\frac{\Omega}{\omega}\right) \int_{\mathcal{D}_9} dk_y g_R^{\text{BCS}}(p_{1x}, -p_{1x}, -k_y) \\ & \times g_R^{\text{BCS}}(k_y, -k_y, p_{3x}), \end{aligned} \quad (\text{C4})$$

$$\begin{aligned} \Gamma_{2R(b)}^{(4)} = & \frac{i}{4\pi^2 v_F} \ln\left(\frac{\Omega}{\omega}\right) \int_{\mathcal{D}_9} dk_y g_R^{\text{BCS}}(p_{1x}, -p_{1x}, k_y) \\ & \times g_R^{\text{BCS}}(-k_y, k_y, p_{3x}), \end{aligned} \quad (\text{C5})$$

for the renormalized one-particle irreducible four-point function in the backscattering and forward-scattering channels.

*eberth@unb.br

- ¹P. W. Anderson, Science **235**, 1196 (1987).
- ²For a review, see J. Voit, Rep. Prog. Phys. **58**, 977 (1995).
- ³E. H. Lieb and F. Y. Wu, Phys. Rev. Lett. **20**, 1445 (1968).
- ⁴R. Shankar, Rev. Mod. Phys. **66**, 129 (1994).
- ⁵J. Gonzalez, F. Guinea, and M. A. H. Vozmediano, Phys. Rev. Lett. **79**, 3514 (1997).
- ⁶D. Zanchi and H. J. Schulz, Phys. Rev. B **61**, 13609 (2000).
- ⁷N. Dupuis, Int. J. Mod. Phys. B **14**, 379 (2000).
- ⁸J. Gonzalez, Phys. Rev. B **63**, 045114 (2001).
- ⁹P. Kopietz and T. Busche, Phys. Rev. B **64**, 155101 (2001).
- ¹⁰P. Kopietz, Nucl. Phys. B **595**, 493 (2001).
- ¹¹J. Gonzalez, Nucl. Phys. B **642**, 407 (2002).
- ¹²B. Binz, D. Baeriswyl, and B. Douçot, Eur. Phys. J. B **25**, 69 (2002).
- ¹³A. A. Katanin and A. P. Kampf, Phys. Rev. B **68**, 195101 (2003).
- ¹⁴T. Baier, E. Bick, and C. Wetterich, Phys. Lett. B **605**, 144 (2005).
- ¹⁵C. J. Halboth and W. Metzner, Phys. Rev. B **61**, 7364 (2000).
- ¹⁶C. Honerkamp, M. Salmhofer, N. Furukawa, and T. M. Rice, Phys. Rev. B **63**, 035109 (2001).

- ¹⁷A. T. Zheleznyak, V. M. Yakovenko, and I. E. Dzyaloshinskii, Phys. Rev. B **55**, 3200 (1997).
- ¹⁸S. Dusuel, F. V. deAbreu, and B. Douçot, Phys. Rev. B **65**, 094505 (2002).
- ¹⁹J. I. Kishine and K. Yonemitsu, Phys. Rev. B **59**, 14823 (1999).
- ²⁰D. Zanchi, Europhys. Lett. **55**, 376 (2001).
- ²¹A. A. Katanin and A. P. Kampf, Phys. Rev. Lett. **93**, 106406 (2004).
- ²²L. Arrachea and D. Zanchi, Phys. Rev. B **71**, 064519 (2005).
- ²³D. Rohe and W. Metzner, Phys. Rev. B **71**, 115116 (2005).
- ²⁴A. Ferraz, Phys. Rev. B **68**, 075115 (2003).
- ²⁵H. Freire, E. Corrêa, and A. Ferraz, Phys. Rev. B **71**, 165113 (2005).
- ²⁶V. Mastropietro, Phys. Rev. B **77**, 195106 (2008).
- ²⁷H. Freire, E. Correa, and A. Ferraz, Phys. Rev. B **78**, 125114 (2008).
- ²⁸For more details about marginally relevant and irrelevant scattering processes as well as for a very thorough review on the Wilsonian RG, see Ref. 4.
- ²⁹C. Honerkamp, M. Salmhofer, and T. M. Rice, Eur. Phys. J. B **27**, 127 (2002).